AD-A189 000 ULTRASONIC-VELOCITY STUDIES OF COMPOSITE AND HETEROGENEOUS MATERIALS(U) COLORADO UNIV AT BOULDER DEPT OF MECHANICAL ENGINEERING S K DATTA ET AL APR 87 1/1

UNCLASSIFIED CUMER-87-1 N00014-86-K-0280 F/G 11/4 NL

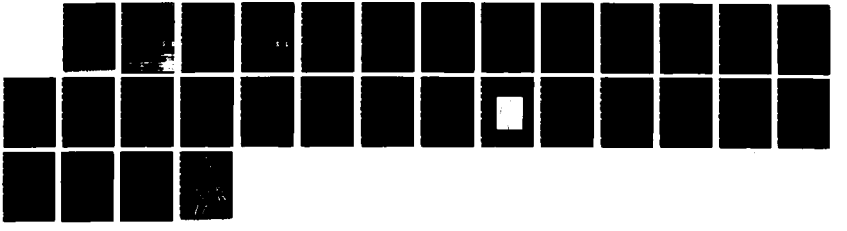

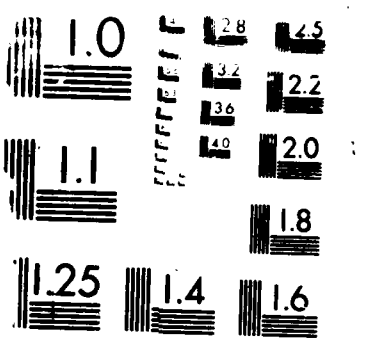

RESOLUTION TEST CHART

UNIVERSITY OF COLORADO

ULTRASONIC-VELOCITY STUDIES OF COMPOSITE AND HETEROGENEOUS MATERIALS

S.K. Datta
University of Colorado and CIRES

H.M. Ledbetter
National Bureau of Standards

A.H. Shah
University of Manitoba

CUMER 87-1 April, 1987

DEPARTMENT OF MECHANICAL ENGINEERING

Contract N00014-86-K-0280

College of Engineering
Boulder, Colorado

ULTRASONIC-VELOCITY STUDIES OF COMPOSITE AND HETEROGENEOUS MATERIALS

Subhendu K. Datta
Department of Mechanical Engineering and CIRES
University of Colorado, Boulder, Colorado 80309

Hassel M. Ledbetter
Fracture and Deformation Division
Institute for Materials Science and Engineering
National Bureau of Standards, Boulder, Colorado 80303

Arvind H. Shah
Department of Civil Engineering
University of Manitoba, Winnipeg, Canada R3T2N2

ABSTRACT

Ultrasonic measurements of wave-propagation characteristics in composite and heterogeneous materials provide an excellent means to study their mechanical properties. In recent years we have studied, both theoretically and experimentally, characteristics of elastic-wave propagation in particle-reinforced composites and heterogeneous materials as well as in homogeneous and laminated fiber-reinforced composites. Comparison of theoretical predictions with obervations of wave velocities has shown good agreement and has provided a way to evaluate microstructural dependence of mechanical properties of these materials. Modeling predictions coupled with observations can also be used to obtain mechanical properties of the reinforcing phase, which are sometimes not easily obtained. In this paper we present results of some of these recent studies.

We also present results of our study of changes in phase velocities and attenuation caused by interface layers between the reinforcing phase and the matrix. We show that this third phase measurably modifies the dispersion behavior. This should lead to effective characterization of interface layer properties by ultrasonic methods.

INTRODUCTION

Determination of effective elastic moduli and damping properties of a heterogeneous or composite material by using elastic waves (propagating and standing) is very effective. Several theoretical studies[1-13] show that for long wavelengths one can calculate the effective wave speeds of plane-longitudinal and plane-shear waves through such a material. At long wavelengths, wave speeds thus calculated are nondispersive; they provide values for the static effective elastic properties. References to other studies can be found in those cited.

We present results of some of our recent studies of phase velocity and attenuation of plane longitudinal and shear waves propagating in a medium with microstructure. Microstructures studied were either inclusions or fibers. In the first case, we examined the effect of inclusion shape, volume fraction, and elastic properties on wave speeds. We studied inclusions with their interface layers separating them from the matrix medium. For fiber-reinforced materials, we studied continuous aligned fibers. In this case, the medium behaves anisotropically because of the alignment of the fibers.

The theoretical model for these microstructural studies used a wave-scattering approach and

(2)

ULTRASONIC-VELOCITY STUDIES OF COMPOSITE AND HETEROGENEOUS MATERIALS

S.K. Datta
University of Colorado and CIRES

H.M. Ledbetter
National Bureau of Standards

A.H. Shah
University of Manitoba

CUMER 87-1 April, 1987

predicted the macroscopic isotropic elastic properties for the case of random orientation of inclusions and for spherical inclusions. For aligned fiber-reinforced materials the model gives the anisotropic elastic properties. The scattering approach led also to an estimation of attenuation and dispersion of waves via the *optical theorem*.

The scattering approach applies to a macroscopically homogeneous medium, infinite in extent. For a bounded medium such as laminated-plate structures we, developed a hybrid numerical technique to analyze dispersion of guided waves. In this paper we present some of our computational results showing the effect on dispersement characteristics caused by interface soft layers between stiff layers in a plate.

The experimental methods[10,14,15] consisted of a pulse-echo technique and a resonance method. These were chosen to provide the advantages of small specimens and low inaccuracy. For details of the experimental techniques, the reader is referred to the references cited.

THEORY

Scattering by a Single Inclusion

Consider a single elastic ellipsoidal inclusion with material properties λ', μ', ρ' embedded in an elastic matrix with properties λ, μ, ρ. Assume that the inclusion is separated from the matrix by a thin layer of elastic material with properties λ_1, μ_1, ρ_1, which are variable through the thickness. Here λ, μ are the Lamé constants and ρ is the density. The geometry of he problem is shown in Figure 1.

We need to find the field scattered by this inclusion when it is excited by an incident elastic wave. A low-frequency approximate solution to this problem was presented earlier[16] for the case of no intermediate layer between the inclusion and the matrix. It can be shown that if the exciting field is given by, dropping the time factor $e^{i\omega t}$,

$$\underset{\sim}{u}^{(E)} = \sum_{n=0}^{\infty} \sum_{m=-n}^{n} \left[a_{mn} \underset{\sim}{L}^{(1)}_{mn}(r,\theta,\phi) + \tau b_{mn} \underset{\sim}{N}^{(1)}_{mn}(r,\theta,\phi) + \tau c_{mn} \underset{\sim}{M}^{(1)}_{mn}(r,\theta,\phi) \right] \tag{1}$$

then the scattered field is

$$\underset{\sim}{u}^{(S)} = \sum_{\nu=0}^{2} \sum_{\mu=-\nu}^{\nu} \left[A_{\mu\nu} \underset{\sim}{L}^{(3)}_{\mu\nu}(r,\theta,\phi) + \tau B_{\mu\nu} \underset{\sim}{N}^{(3)}_{\mu\nu}(r,\theta,\phi) \right] + O(\epsilon^4) \tag{2}$$

Here $\underset{\sim}{L}^{(1)}_{mn}$, $\underset{\sim}{N}^{(1)}_{mn}$, and $\underset{\sim}{M}^{(1)}_{mn}$ are spherical vector wave functions[17] that are finite at $r = 0$ and $\underset{\sim}{L}^{3}_{mn}$, $\underset{\sim}{N}^{3}_{mn}$ are those that satisfy the radiation condition as $r \to \infty$. The constants $A_{\mu\nu}$ and $B_{\mu\nu}$ are given by[13]

$$A_{\mu\mu} = \frac{iv_0\epsilon^3}{4\pi c^3} \sum_{\nu_1} \sum_{\mu_1'=-\nu_1}^{\nu_1} \hat{T}^{\mu_1\nu_1}_{\mu\nu} \left[a_{\mu_1'\nu_1} + \delta(\nu) b_{\mu_1'\nu_1} \right],$$

$$B_{\mu\mu} = \frac{iv_0\epsilon^3}{4\pi c^3} \sum_{\nu_1} \sum_{\mu_1'=-\nu_1}^{\nu_1} \Delta(\nu)\ \hat{T}^{\mu_1\nu_1}_{\mu\nu} \left[a_{\mu_1'\nu_1} + \delta(\nu) b_{\mu_1'\nu_1} \right], \tag{3}$$

where v_0 is the volume of the ellipsoid and

$$\epsilon = k_1 C,\ k_1 = \omega/C_1,\ \tau = C_1/C_2$$

$$\delta(\nu) = \begin{cases} 3\tau^2, & \nu=0,2 \\ 2\tau, & \nu=1 \end{cases}$$

$$\Delta(\nu) = \begin{cases} \tau^2, & \nu=1 \\ \frac{\tau^3}{2}, & \nu=0,2 \end{cases}$$

C_1 and C_2 are the longitudinal and shear wave speeds in the matrix medium. Expressions for $\hat{T}^{\mu_1\nu_1}_{\mu\nu}$, can be found elsewhere[9].

Effective Properties of a Composite Medium with Inclusions

Once the scattered field caused by a single inclusion is known, multiple scattering from a number of inclusions can be easily calculated. In particular, for a random homogeneous distribution of ellipsosidal inclusions

$$\frac{C^{(2)}}{C_1^{*2}} = \left[(1+9\bar{c}P_1)(1-3\bar{c}P_0)\left[1+\frac{3}{2}\ \bar{c}P_2(2+3\tau^2)\right] \right] / (1-15\bar{c}P_2(1+3\bar{c}P_0) + \frac{3}{2}\bar{c}P_2(2+3\tau^2), \tag{4}$$

$$\frac{C^2}{C_2^{*2}} = \frac{(1+9\bar{c}P_1)\left[1+\frac{3\bar{c}}{2}P_2(2+3\tau^2)\right]}{1+\frac{3c}{4}P_2\ (4-9\tau^2)}. \tag{5}$$

Here $\bar{c} = \frac{4}{3\pi abcn_0}$, n_0 being the number density of inclusions. The constants P_0 and P_2 depend on the geometrical properties of the inclusions as well as on the mechanical properties $(\lambda,\mu,\lambda',\mu')$ of the matrix and the inclusions. P_1 is simply given by

$$P_1 = \frac{\rho'/\rho - 1}{9}.$$

In deriving (4) and (5) it has been assumed that the inclusions are similar in shape, size and physical properties.

When there is an intermediate layer between the inclusion and the matrix, then the coefficients $A_{\mu\nu}$ and $B_{\mu\nu}$ cannot be obtained in exact form; they have to be determined numerically for general ellipsoidal inclusions. For spherical inclusions, on the other hand, exact expressions for $A_{\mu\nu}$ and $B_{\mu\nu}$, valid at arbitrary frequencies, can be obtained if the intermediate layer has constant properties. Also, for spherical inclusions with *thin* interface layers having variable properties, $A_{\mu\nu}$ and $B_{\mu\nu}$ can be obtained[18] approximately if $h/\lambda<<1$, $h/a<<1$. Here h is the thickness of the interface layer, a the radius of the spherical inclusions, and λ the wavelength of the incident wave. Even then, the problem of determining phase velocities of longitudinal and shear waves in the composite material at finite frequencies is complicated[6]. The problem is simpler if the volume concentration of inclusions is small. This is discussed in the following

Consider a spherical inclusion of radius a with an interface layer (Figure 2). Let the incident field be given by

$$\underset{\sim}{u}^{i} = e^{ik_1 z}\,\underset{\sim}{e}_z + e^{ik_2 z}\,\underset{\sim}{e}_x \tag{6}$$

where $k = \omega/C_2$. The scattered field is then given by

$$\underset{\sim}{u}^{(s)} = \underset{\sim}{u}^{p} + \underset{\sim}{u}^{s} \tag{7}$$

where superscripts p and s refer to longitudinal-wave and shear-wave components, respectively. Now it will be assumed that within the interface layer the elastic coefficients λ_1 and μ_1 vary with the distance from the center of the inclusions as

$$\begin{aligned} &\lambda_1(r) + 2\mu_1(r) = (\lambda_1' + 2\mu_1')\, f(r), \quad a<r<a+h, \\ &\mu_1(r) = \mu_1'\, g(r), \quad a<r<a+h, \end{aligned} \tag{8}$$

where f(r) and g(r) are general integrable functions of r. If it is further assumed that $h/a<<1$, $h/\lambda<<1$, then it can be shown that the displacement components satisfy the approximate boundary conditions on r = a.

$$\begin{aligned} u_r^{(s)} + u_r^{(i)} - u_r^{(t)} &= \frac{hK_1}{\lambda_1'+2\mu_1'}\,\tau_{rr}^{(t)} \\ u_\theta^{(s)} + u_\theta^{(i)} - u_\theta^{(t)} &= \frac{hK_2}{\mu_1'}\,\tau_{r\phi}^{(t)} \end{aligned} \tag{9}$$

$$u_{\phi}^{(s)} + u_{\phi}^{(i)} - u_{\phi}^{(t)} = \frac{hK_2}{\mu_1} \tau_{r\phi}^{(t)}$$

where

$$K_1 = \int_0^1 \frac{dx}{f(a+hx)}, \quad K_2 = \int_0^1 \frac{dx}{g(a+hx)}$$

Superscript (t) refers to the field quantities within the inclusion. τ_{ij} is the stress tensor. To this order of approximation the traction components τ_{rr}, $\tau_{r\theta}$ and $\tau_{r\phi}$ are continuous at r = a. These simplified boundary conditions allow the single scattering problem to be solved exactly[18].

When $r \to \infty$, one obtains from Eq. (7) the far-field behavior of $\underset{\sim}{u}^s$ when the incident wave is given by a plane-longitudinal wave (the first term on the right-hand side of Eq. (6)). Then it can be shown that

$$\underset{\sim}{u}^p \sim g^p(\theta) \frac{e^{ik_1 r}}{r} \underset{\sim}{e}_r, \quad \underset{\sim}{u}^s \sim h^p(\theta) \frac{e^{ik_2 r}}{r} \underset{\sim}{e}_\theta \tag{10}$$

For the incident plane-shear wave (the second term on the right hand side of Eq. (6)) one finds

$$\underset{\sim}{u}^p \sim g^p(\theta,\phi) \frac{e^{ik_1 r}}{r} \underset{\sim}{e}_r \tag{11}$$

$$\underset{\sim}{u}^s \sim h_1^s(\theta,\phi) \frac{e^{ik_2 r}}{r} \underset{\sim}{e}_\theta + h_2^s(\theta,\phi) \frac{e^{ik_2 r}}{r} \underset{\sim}{e}_\phi .$$

The expressions for the amplitude functions g^p, h^p, and so on, can be obtained from our earlier study[18]. Using Eqs. (10) and (11) and the forward-scattering theorem[19] we then obtain the equations for the effective wave numbers in the composite medium:

$$\frac{k_1^{*2}}{k_1^2} = 1 + \frac{4\pi}{k_1^2} n_0 g^p(0) \tag{12}$$

for the longitudinal wave and

$$\frac{k_2^{*2}}{k_2^2} = 1 + \frac{4\pi}{k_2^2} n_0 h_1^s(0,0) \tag{13}$$

for the shear wave. Since $g^p(0)$ and $h_1^s(0,0)$ are complex, effective waves will be both dispersive

and attenuative.

Effective Properties of a Fiber-Reinforced Composite

The analysis presented above for inclusions can be applied also to a medium reinforced by aligned continuous fibers. In that case, one can derive equations similar to (4) and (5) for longitudinal and shear waves propagating perpendicular to the fibers. Taking the x_3 axis along the fibers, and assuming them to be transversely isotropic about this axis, it was shown[20] that for SH waves polarized along the fibers the effective wave number, β^*, is

$$\frac{\beta^{*2}}{k_2^2} = \frac{\rho^*(1-\bar{c}(m-1)/(m+1))}{\rho\ (1+c(m-1)/(m+1))} \quad . \tag{14}$$

where ρ^* is the effective density and $m = C_{44}/\mu$. For longitudinal and shear waves polarized in a plane perpendicular to the fibers we get

$$\frac{k_1^{*2}}{k_1^2} = \frac{\rho^*(1+\bar{c}P_0)[1+\bar{c}P_2(1+\tau^2)]}{1-cP_2(1-\tau^2)-2c^2P_0P_2} \quad , \tag{15}$$

$$\frac{k_2^{*2}}{k_2^2} = \frac{\rho^*/\rho}{1+\dfrac{2\bar{c}(C_{66}-\mu)(\lambda+2\mu)}{2\mu(\lambda+2\mu)+(1-c)(\lambda+3\mu)(C_{66}-\mu)}} \quad . \tag{16}$$

Note that C_{11}, C_{33}, C_{44}, C_{66}, and C_{13} are the five independent elastic constants characterizing the fibers and $\rho = \rho[1+c(\rho'/\rho-1)]$. P_0 and P_2 are defined by the relationships

$$P_0 = -\frac{K'_T - (\lambda+\mu)}{K'_T+\mu}, \quad P_2 = -\frac{\mu(C_{66}-\mu)}{C_{66}(\lambda+3\mu)+\mu(\lambda+\mu)} \quad . \tag{17}$$

where K'_T is the plane-strain bulk modulus of the fibers. The remaining two elastic moduli of the composite are obtained from relationships derived by Hill[21].

Dispersion of Guided Waves in a Laminated Plate with Interface Layers

In composite materials, interfaces between the different constitutents play an important role in determining their mechanical behavior. As discussed above, the effect of interfacial layers between inclusions and matrix medium on composite properties can be evaluated approximately using a scattering approach. For laminated-composite plate structures, the effect on the dispersion characteristics caused by interfacial layers between the laminae can be analyzed in detail. The changes in dispersion characteristics should provide a way to ultrasonically evaluate the interface properties.

In this section we briefly outline a theoretical technique to study guided-wave propagation in a laminated plate with interface layers. For simplicity of analysis, we consider only isotropic laminae and isotropic interface layers. Equations governing guided-wave propagation in such a

plate can be solved exactly. However, if the laminae are isotropic, then an exact analysis is extremely complicated. To avoid the difficulties associated with an exact analysis, we developed a stiffness method in which each lamina (and interface layer) is divided into several sublayers. Polynomial interpolation functions for through-thickness variation of displacements in each layer are assumed. The interpolation functions involve a discrete number of generalized coordinates that are functions of the in-plane coordinates x and y (Figure 3) and time t. The generalized coordinates are the displacements and tractions at the interfaces between the adjoining sublayers, thus ensuring continuity of these quantities at the interfaces. By applying Hamilton's principle the dispersion equation is obtained as a standard algebraic eigenvalue problem whose solutions yield the dispersion relations and the variation of stresses and displacements through the plate thickness of the plate. This technique was used earlier[22] to study wave propagation in an infinite periodically laminated medium. The application of the technique to a sandwich plate was discussed in detail elsewhere[23]. Here, for brevity, we present only the results for a particular sandwich plate.

RESULTS AND DISCUSSION

Cast-Iron Elastic Constants

Graphite-particle shape affects cast-iron's properties, both physical and mechanical. Several studies[24-27] dealt with the various properties of cast-iron as they depend on graphite particle shape. But all these studies, experimental and theoretical, dealt only with limiting shapes: sphere, rod, and disc. They failed to deal with arbitrary aspect ratio, c/a, of the particles. Using Eqs. (4) and (5), we calculated Young's modulus, E, of cast-iron for various values of c/a. The results are shown in Figure 4 along with the experimental observations reported by various investigators [24-26]. In this figure, calculated results are for two different volume fractions--10 and 12 percent--a range that contains most of the studied cast-irons.

The two upper, nearly horizontal, curves correspond to graphite's upper third-order elastic-constant bounds. The two lower curves correspond to the lower bounds. From monocrystal elastic constants, using equations by Kröner and Koch[28], for graphite, Wawra, et al[29] calculated third-order elastic-constant bounds. They found the following effective quasi-isotropic elastic constants: $E' = 4.17(1.34)$ GPa; $\mu' = 1.41(0.45)$ GPa. Values outside parentheses denote upper bounds; those inside denote lower. For the matrix phase we took the constants for alpha iron: $E = 206$ GPa, $\mu = 80.0$ GPa.

Corresponding to observation, our model predicts a strong dependence of Young's modulus on aspect ratio. Near the spherical limit (c/a = 1), E^* varies slowly with c/a. Near the oblate-disc limit (c/a = 0), E^* varies rapidly with c/a. An interesting result is that graphite's lower-bound quasi-isotropic elastic constants fit observation so well.

Elastic Constants of Graphite-Aluminum Composite

Figure 5 shows the microstructure of graphite-fiber-reinforced aluminum obtained from a commerical source. By Archimedes' method, we found the mass density of the composite to be 2.013 g/cm^3. For a fiber volume fraction of 0.70, using 2.6523 for aluminum, the graphite fiber density is predicted to be 1.738, very close to the manufacturer's estimate of 1.76.

We determined the nine C_{ij} by measuring eighteen sound speeds on four specimen geometries described previously[30]. For brevity, we omit further description, except for a few salient details: bond--phenylsalicylate; transducers--quartz, x-cut and ac-cut; frequencies--5 to 6 MHz; specimen size--16-mm cube, or smaller depending on specimen geometry.

Table I shows the study's principal results. Column 1 lists various elastic constants. Column 2 gives a set of fiber elastic constants[31,32]. We chose these because E_{33} agrees closely with the E_{33} for the present fiber. Column 3 shows measured results. From the measured results and the predictions from Eqs. (14)-(16) together with Hill's relationships, we predicted the fiber properties shown in column 4. We used the calculational sequence: C_{44}, C_{66}, C_{11},-C_{66}, ν_{31}, and E_{33}. Column 5 shows the calculated C_{ij}. Finally, column 6 shows the ratio of column 5 to column 3.

Results of column 3 of Table I show that the studied composite shows orthotropic elastic symmetry, which is approximately transversely isotropic with the x_3-axis as the symmetry axis. The microstructure in Figure 5 also suggests transverse-isotropic symmetry.

Concerning the first-guess graphite-fiber elastic-constant calculations, we find reasonable agreement for C_{11}, C_{22}, C_{33}, and C_{66}. Thus, the criterion of choosing a graphite elastic-constant set based on E_{33}, the axial Young's modulus, succeeds partially.

One can obtain a better, complete graphite elastic-constant set by using the model equations inversely. This is shown in column 4 and it is seen that the constants appearing in this column differ significantly from the first-guess values in column 2.

For the graphite-aluminum composite, Figure 6 shows the variation with temperature of the principal elastic stiffnesses C_{ij} (i = 1,6). For comparison, the figure also shows the temperature variation of the longitudinal and shear moduli of the aluminum matrix. The graphite-aluminum C_{ij}-versus-temperature results in Figure 6 show strong anisotropy. The largest change occurs in C_{11}, the longitudinal elastic stiffness perpendicular to the fibers. The smallest change occurs in C_{33}, the longitudinal elastic stiffness parallel to the fibers. These changes agree with the well-known high axial elastic stiffness and low axial thermal expansivity of graphite fibers. The three shear moduli--C_{44}, C_{55}, C_{66}--fall between these extremes. Among the shear moduli, C_{66} shows the largest change; this reflects the low C_{66} values for both the fiber and the matrix. Almost universally, lower elastic stiffness, C, means higher dC/dT. In Figure 6, the near equivalence of dC_{44}/dT and dC_{55}/dT reflects the approximate transverse isotropy of this composite.

Interface Effects on Damping and Phase Velocities in an SiC-Particle Reinforced Aluminum

Equations (12) and (13) provide implicit relations for the complex wave numbers k_1^* and k_2^* if it is assumed that the inclusion is placed in a composite medium with the effective unknown dynamic properties. Then k_1^2 and k_2^2, appearing on the right-hand sides of Eqs. (12) and (13) will be replaced by k_1^2 and k_2^2 respectively. These equations then can be solved iteratively for the unknown k_1^* and k_2^*. These results are shown in Figures 7-10. Note that $Im(k^*)$ measures damping and $Re(k^{/k})$ measures the ratio of the phase velocities in the matrix and the composite. In these calculations the interface layer properties were assumed to vary linearly across the layer thickness from the properties of the particles to those of the matrix. The elastic properties of the particles and the matrix were taken as: $\lambda'+2\mu' = 4.742\text{x}10^{11}$ N/m^2, $\mu' = 1.881\text{x}10^{11}$ N/m^2, $\rho' = 3.181$ g/cm^3, $\lambda+2\mu = 1.105\text{x}10^{11}$ N/m^2, $\mu = 0.267\text{x}10^{11}$ N/m^2, $\zeta = 2.705$ g/cm^3. Calculations were performed with or without interface layers and at two volume fractions: c = 0.05, 0.15. The presence of the interface layer decreases the damping as well as the phase velocities.

Dispersion in a Sandwich Plate with Low-Velocity Interface Layers

Using the numerical technique described in the theory section, we analyzed the dispersion of elastic waves in the five-layer plate shown in Figure 3. The displacement is assumed to be

$$\underset{\sim}{u}(x,z,t) = \underset{\sim}{f}(z)e^{i(kx-\omega t)} \tag{18}$$

If all the layers are transversely isotropic with the symmetry axes parallel or perpendicular to the direction of wave propagation (x-axis), then the equations governing the y-component of the displacement, u_y, uncouple from those governing the x and z components. The former correspond to the SH motion and the latter to plane strain motion.

Figures 11 and 12 show the disperison curves for the plane-strain motion, and Figure 13 shows those for the SH motion. In these figures the vertical axis corresponds to $\Omega = \omega h_1/\pi\sqrt{\mu_1/\zeta}$ and the horizontal axis to $\zeta = kh/\pi$. Here h is the thickness of each of the two low velocity layers and $C_2 = \sqrt{\mu/\sigma}$ is the shear wave velocity in these layers. The properties of the stiff layers are taken to be $\mu' = 8.76\times10^9$ N/m^2, $\rho' = 1.771$ g/cm^3, $\nu' = 0.3$. Those of the soft layers are $\mu = 1.77\times10^9$ N/m^2, $\rho = 1.2$ g/cm^3, $\nu = 0.3$. h/H is taken to be 0.1

Figure 11 shows the first nine modes for small values of Ω and ζ. It is seen that these dispersion curves look qualitatively very similar to those for an isotropic plate. However, the important difference is that cut-off frequencies of higher modes are lowered significantly. Figure 12 shows the first three modes over a wide range of frequency and wave number. It is found that at short wavelengths the phase velocity of the first two modes departs significantly from the Rayleigh wave velocity in the stiff layer. Dispersion curves for SH-motion (Figure 13) also show similar features. The departure depends on the ratios of the elastic properties and of the thicknesses of the low-velocity layers and the laminae. This effect and the lowering of cutoff frequencies should lead to ultrasonic characterization of interfaces.

CONCLUSIONS

We have shown that modeling and experimental observations of particle-reinforced and fiber-reinforced materials lead to property characterization of the reinforcing phases. Also, we have presented model calculations of interface effects on phase velocities and attenuation of waves in a composite medium. It is shown that, for the particular systems considered, the presence of low-velocity interface layers decreases the phase velocities as well as the attenuation.

ACKNOWLEDGMENT

This study was supported in part by a grant from the Solid Mechanics Division (Program Manager, Dr. Y. Rajapakse) of the Office of Naval Research (ONR-00014-86-K0280), a grant from the National Science Foundation (MSM-8609813), and a grant from the Natural Science and Engineering Research Council of Canada (A-7988). Support was also received from the Office of Nondestructive Evaluation, NBS.

REFERENCES

1. Bose, S.K. and Mal, A.K., "Elastic Waves in a Fiber-Reinforced Composite," *Journal of the Mechanics and Physics of Solids*, Vol. 22, 1974, pp. 217-229.

2. Mal, A.K. and Bose, S.K., "Dynamic Moduli of a Suspension of Imperfectly Bonded Spheres," *Proceedings of the Cambridge Philosophical Society*, Vol. 76, 1974, pp. 587-600.

3. Datta, S.K., "A Self-Consistent Approach to Multiple Scattering of Elastic Waves," *Journal of Applied Mechanics, Transactions of ASME*, Vol. 44, 1977, pp. 657-662.

4. Devaney, A.J., "Multiple Scattering Theory for Discrete, Elastic, Random Media," *Journal of Mathematical Physics*, Vol. 21, 1980, pp. 2603-2611.

5. Berryman, J.G., "Long-Wavelength Propagation in Composite Elastic Media--I. Spherical Inclusions," *Journal of the Acoustical Society of America*, Vol. 68, 1980, pp. 1809-1819.

6. Berryman, J.G., "Long-Wavelength Propagation in Composite Elastic Media--II. Ellipsoidal Inclusions," *Journal of the Acoustical Society of America*, Vol. 68, 1980, pp. 1820-1831.

7. Willis, J.R., "A Polarization Approach to the Scattering of Elastic Waves--II. Multiple Scattering from Inclusions," *Journal of the Mechanics and Physics of Solids*, Vol. 28, 1980, pp. 307-327.

8. Varadan, V.K., Ma, Y., and Varadan, V.V., "A Multiple Scattering Theory for Elastic Wave Propagation in Discrete Random Media," *Journal of the Acoustical Society of America*, Vol. 77, 1985, pp. 375-385.

9. Ledbetter, H.M. and Datta, S.K., "Effective Wave Speeds in an SiC-particle-reinforced Al Composite," *Journal of the Acoustical Society of America*, Vol. 79, 1986, pp. 239-248.

10. Read, D.T. and Ledbetter, H.M., "Elastic Properties of a Boron-Aluminum Composite at Low Temperature," *Journal of Applied Physics*, Vol. 48, 1977, pp. 2827-2831.

11. Kinra, V.K., Petraitis, M.S., and Datta, S.K., "Ultrasonic Wave Propagation in a Random Particulate Composite," *International Journal of Solids and Structures*, Vol. 16, 1980, pp. 301-312.

12. Datta, S.K. and Ledbetter, H.M., "Anisotoropic Elastic Constants of a Fiber-reinforced Boron-Aluminum Composite," *Mechanics of Nondestructive Testing*, W.W. Stinchcomb, ed., Plenum, New York, 1980, pp. 215-230.

13. Ledbetter, H.M. and Datta, S. K., "Young's Modulus and the Internal Friction of an SiC-Particle-Reinforced Aluminum Composite," *Materials Science and Engineering*, Vol. 67, 1984, pp. 25-30.

14. Ledbetter, H.M., "Dynamic Elastic Modulus and Internal Friction in Fibrous Composites," *Non-metallic Materials and Composites at Low Temperatures*, Plenum, New York, 1979, pp. 267-281.

15. Ledbetter, H.M., Frederick, N.V., and Austin, M.W., "Elastic-Constant Variability in

Stainless Steel," *Journal of Applied Physics*, Vol. 51, 1980, pp. 305-309.

16. Datta, S.K., "Diffraction of Plane Elastic Waves by Ellipsoidal Inclusions," *Journal of the Acoustical Society of America*, Vol. 61, pp. 1432-1437.

17. Stratton, J.A., *Electromagnetic Theory*, 1941, McGraw-Hill, New York.

18. Datta, S.K. and Ledbetter, H.M., "Effect of Interface Properties on Wave Progagation in a Medium with Inclusions," *Mechanics of Material Interfaces*, A.P.S. Selvadurai and G.Z. Voyiadjis, eds., Elsevier, The Netherlands.

19. Gubernatis, J.E. and Domany, E., "Effects of Microstructure on the Speed and Propagation of Elastic Waves," *Wave Motion*, Vol. 6, 1984, pp. 579-589.

20. Datta, S.K., Ledbetter, H.M. and Kriz, R.D., "Calculated Elastic Constants of Composites containing Anisotropic Fibers," *International Journal of Solids and Structures*, Vol. 20, 1984, pp. 429-438.

21. Hill, R., "Theory of Mechanical Properties of Fibre-Strenghtened Materials: - I. Elastic Behavior," *Journal of the Mechanics and Physics of Solids*, Vol. 12, 1964, pp. 199-212.

22. Shah, A.H. and Datta, S.K., "Harmonic Waves in a Periodically Laminated Medium," *International Journal of Solids and Structures*, Vol. 18, 1982, pp. 397-410.

23. Datta, S.K., Shah, A.H., Bratton, R.L., and Al-Nassar, Y.N., "Guided Wave Propagation in Laminated Composite Plates with Low-Velocity Interface Layers," to be published.

24. Okamoto, T., Kagawa, A., Kiyoshi, K., and Matsumoto, H., "Effects of Graphite Shape on Thermal Conductivity, Electrical Resistivity, Damping Capacity and Young's Modulus of Cast Iron below 500 degrees 'C.," *Journal of the Japan Foundrymen's Society*, Vol. 55, 1983, pp. 32-36.

25. Löhe, D., Vöhringer, O., and Macherauch, E., "Der Einfluß der Graphitform auf den Elastizitatsmodul von Ferritischen Gußeisen-Werkstoffen," *Zeitschrift fur Metallkunde*, Vol. 74, 1983, pp. 265-273.

26. Speich, G.R., Schwoeble, A.J., and Kapadia, B.M., "Elastic Moduli of Gray and Nodular Cast Iron," *Journal of Applied Mechanics, Transactions of ASME*, Vol. 47, 1980, pp. 821-826.

27. Anand, L., "Elastic Moduli of Gray and Ductile Cast Irons," *Scripta Metallurgica*, Vol. 16, 1982, pp. 173-177.

28. Kröner, E. and Koch, H., "Effective Properties of Disordered Materials," *SM Archives*, Vol. 1, 1976, pp. 183-238.

29. Wawra, H., Gairola, B.K.D., and Kröner, E., "Comparison between Experimental Values and Theoretical Bounds for the Elastic Constants E, G, K and μ of Aggregrates of Noncubic Crystallites," *Zeitschrift fur Metallkunde*, Vol. 73, 1982, pp. 69-71.

30. Ledbetter, H.M. and Read, D.T., "Orthorhombic elastic constants of an NbTi/Cu Composite Superconductor," *Journal of Applied Physics*, Vol. 48, 1977, pp. 1874-1879.

31. Kriz, R.D. and Stinchcomb, W.W., "Elastic Moduli of Transversely Isotropic Graphite Fibers and their Composites," *Experimental Mechanics*, Vol. 19, 1979, pp. 41-49.

32. Smith, R.E., "Ultrasonic Elastic Constants of Carbon Fibers and Their Composites," *Journal of Applied Physics*, Vol. 43, 1972, pp. 2555-2561.

Table 1. Measured and calculated elastic constants for graphite-fiber-reinforced composite and calculated graphite-fiber elastic constants. Except for dimensionless ν_{ij}, units are GPa.

	Fiber[32]	Composite Measured	Fiber Calculated	Composite Calculated	Composite-Calc./Meas.
C_{11}	20.02	32.18	19.09	32.18	1.00
C_{22}	20.02	32.03	19.09	32.14	1.00
C_{33}	234.77	192.24	234.99	194.14	1.00
C_{44}	24.00	21.66	19.94	21.66	1.00
C_{55}	24.00	21.51	19.94	21.66	1.01
C_{66}	5.02	9.31	5.60	9.31	1.00
C_{12}	9.98	13.55	7.89	13.56	1.00
C_{13}	6.45	16.65	10.34	16.60	1.00
C_{23}	6.45	16.65	10.34	16.60	1.00
E_{11}	15.00	25.94	15.66	25.96	1.00
E_{22}	15.00	25.81	15.66	25.96	1.01
E_{33}	232.00	180.09	227.07	180.09	1.00
ν_{12}	0.494	0.396	0.399	0.394	0.99
ν_{13}	0.014	0.052	0.026	0.052	1.00
ν_{23}	0.014	0.053	0.026	0.052	0.98
ν_{21}	0.494	0.394	0.399	0.394	1.00
ν_{31}	0.215	0.363	0.383	0.393	1.00
ν_{32}	0.215	0.366	0.383	0.363	0.99

List of Figures

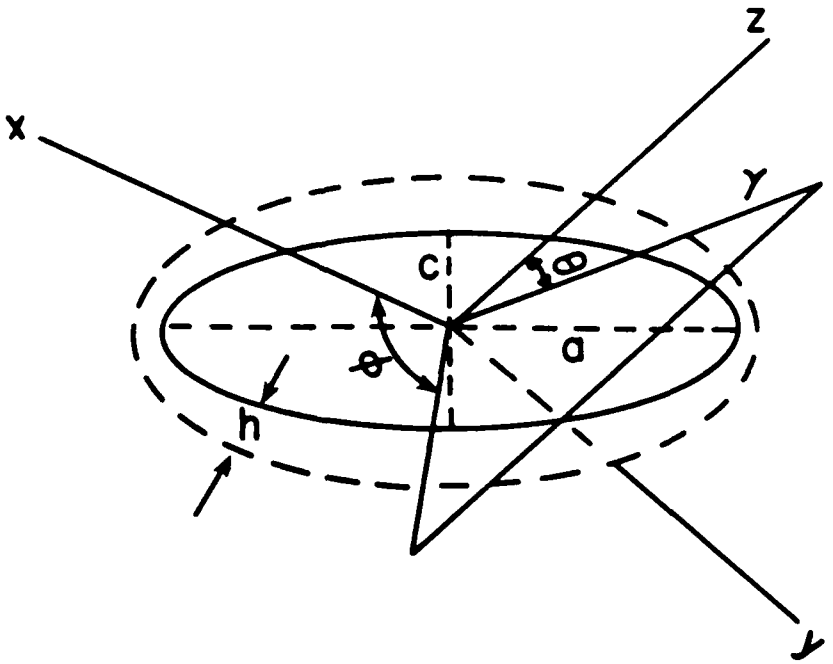

Figure 1

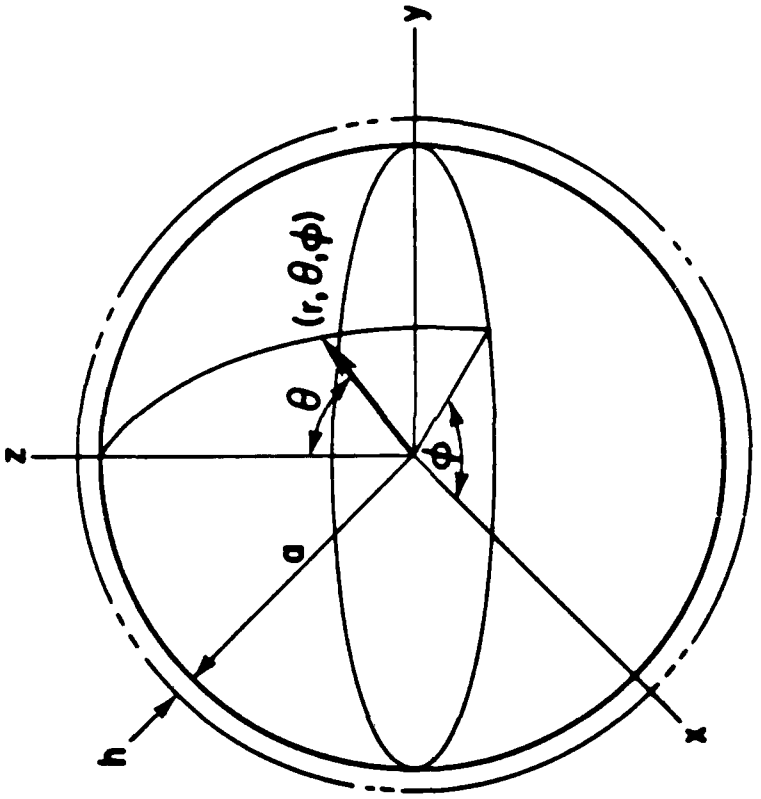

Figure 2

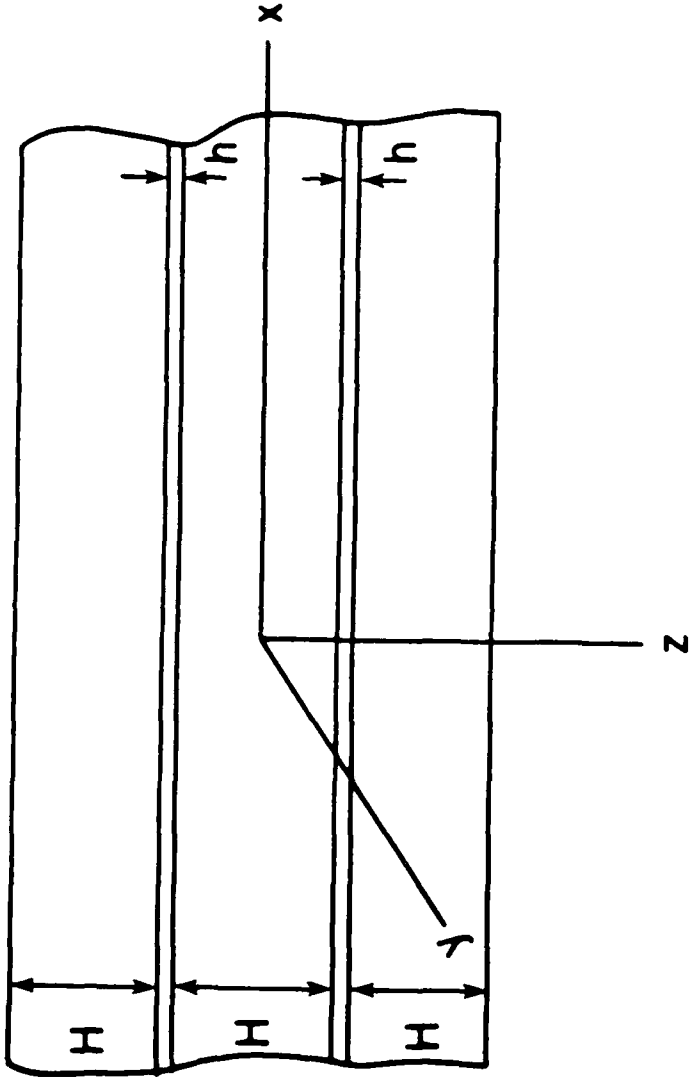

Figure 3

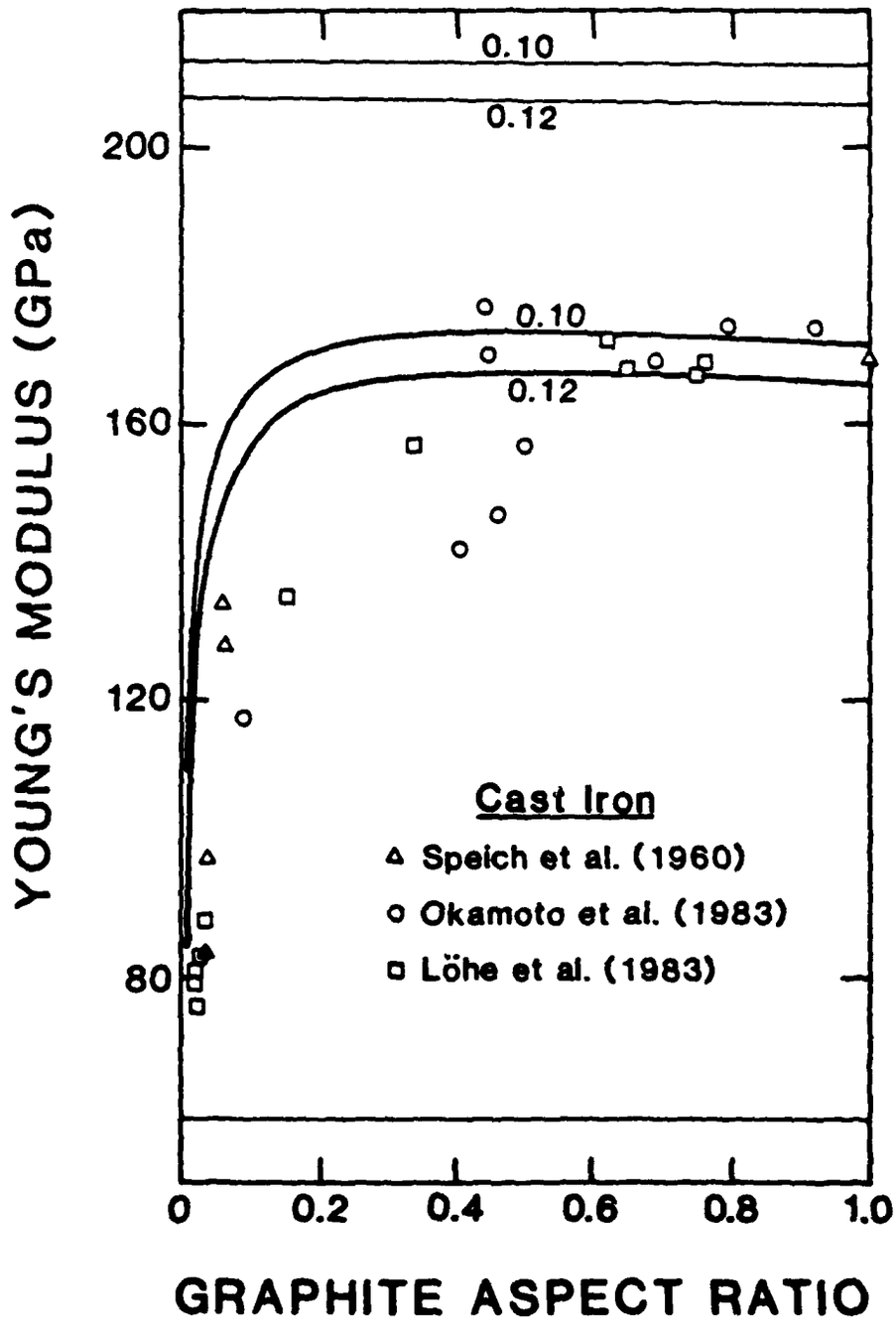
0.10
0.12
200
0.10
0.12
160
120
80
Cast Iron
Speich et al. (1960)
Okamoto et al. (1983)
Löhe et al. (1983)
YOUNG'S MODULUS (GPa)
0
0.2
0.4
0.6
0.8
1.0
GRAPHITE ASPECT RATIO

Figure 4

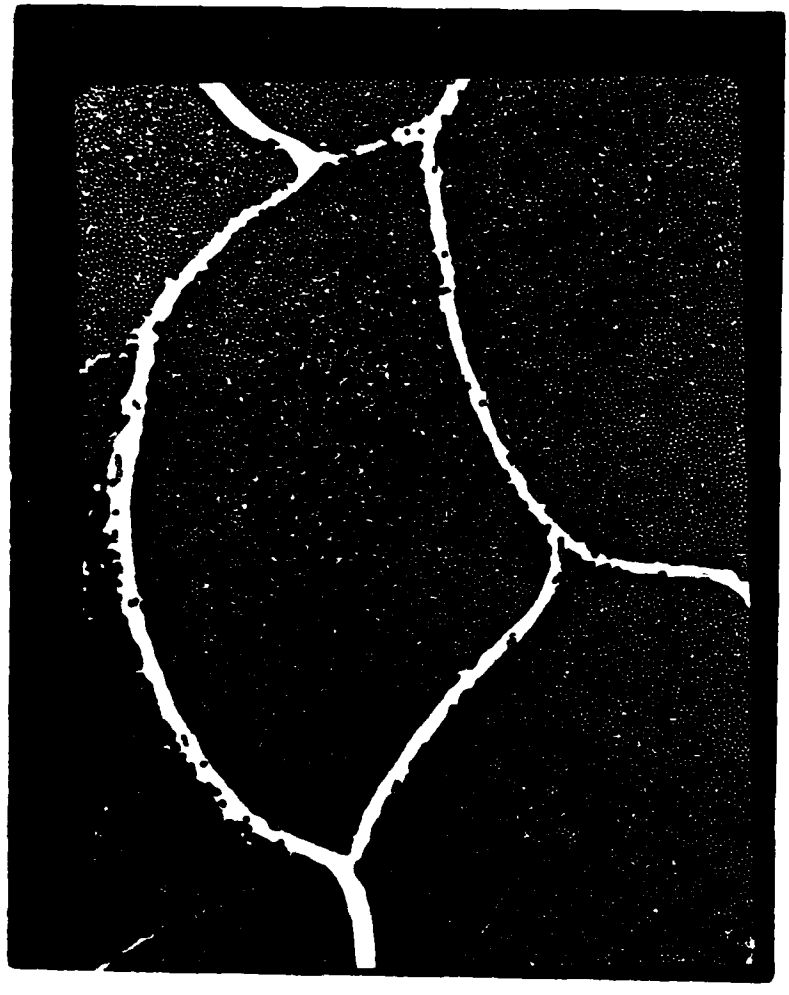

Figure 5

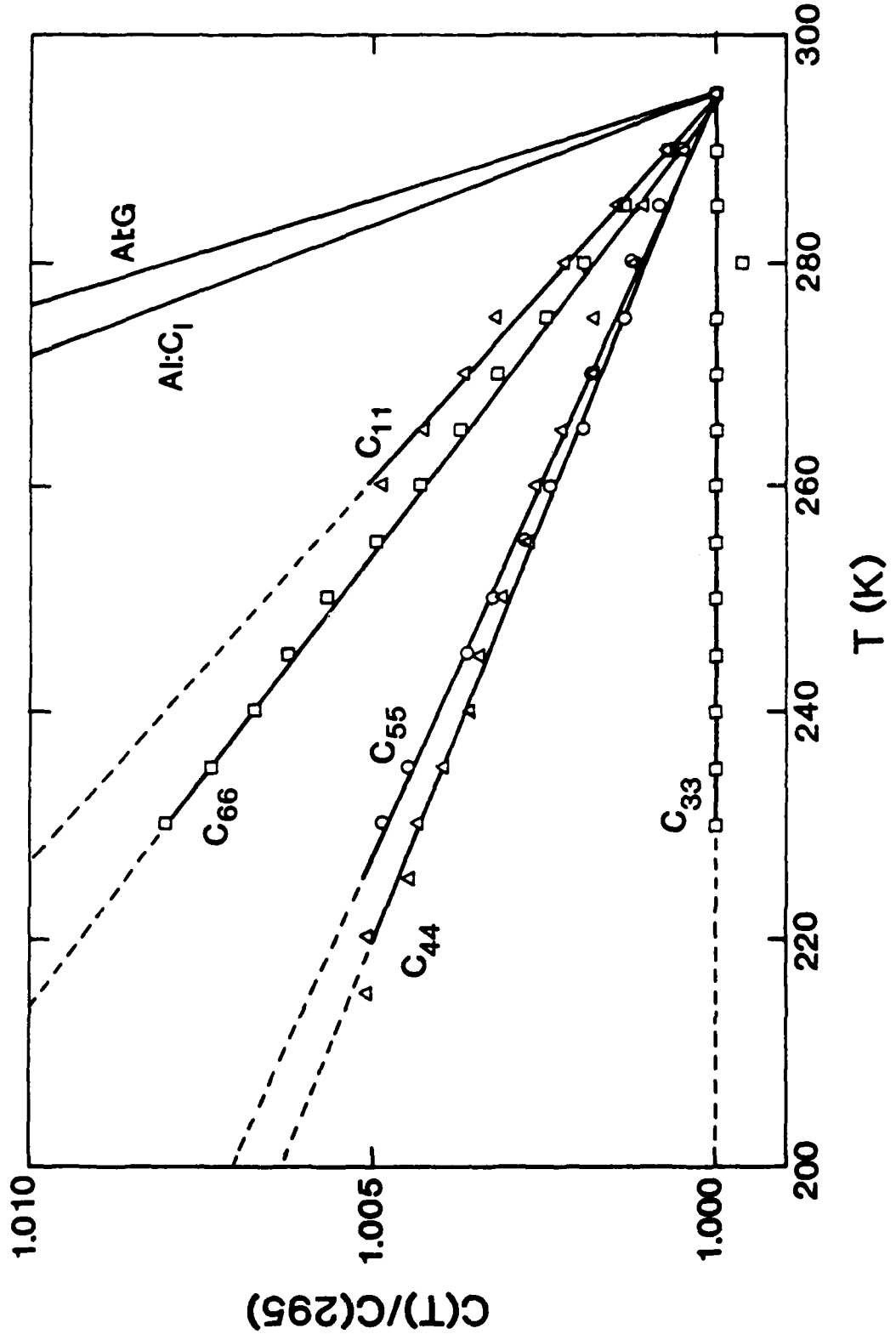
AtG
Al:C$_I$
C$_{11}$
C$_{66}$
C$_{55}$
C$_{44}$
C$_{33}$
1.010
1.005
1.000
C(T)/C(295)
200
220
240
260
280
300
T (K)

Figure 6

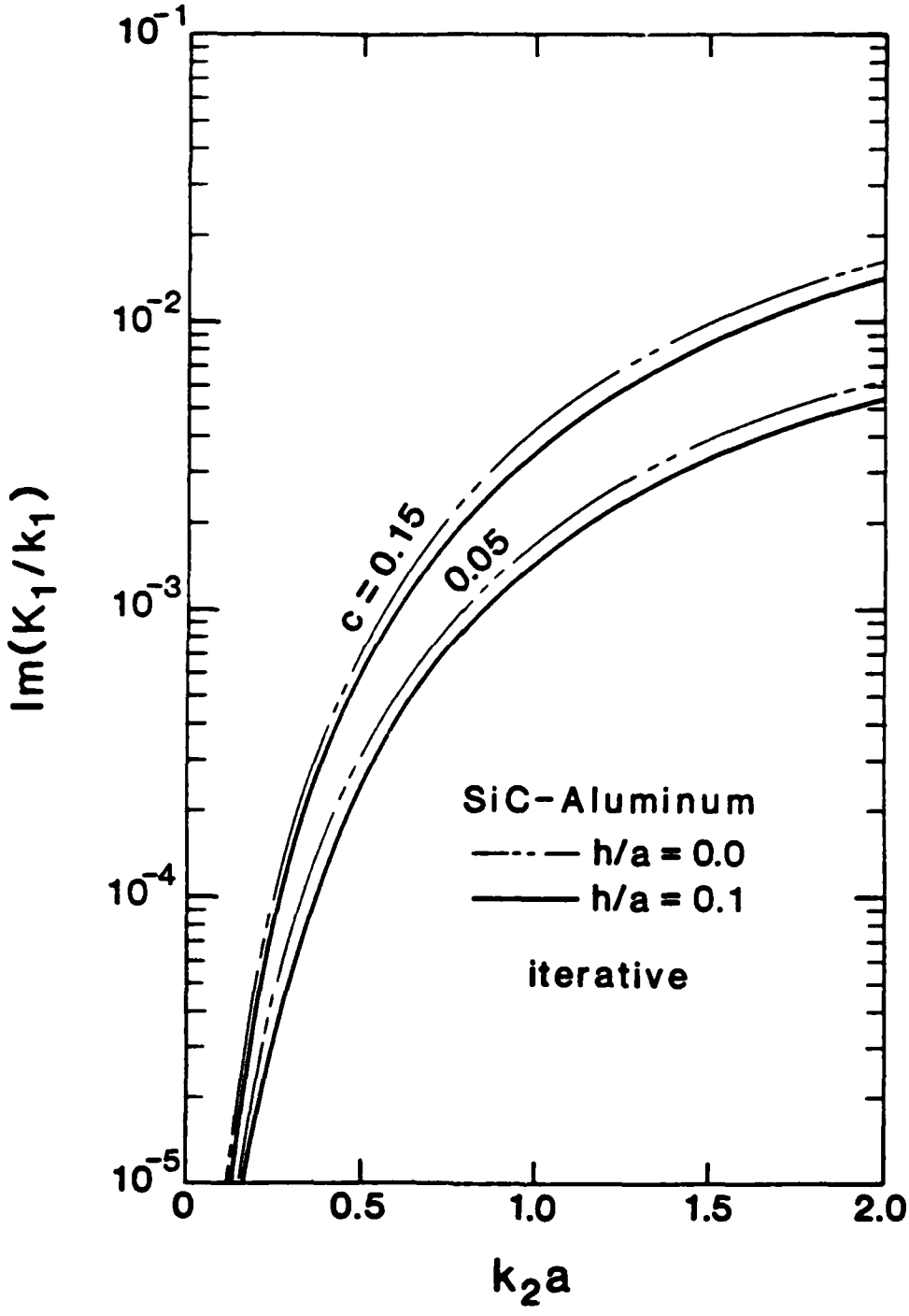
10^{-1}
10^{-2}
10^{-3}
10^{-4}
10^{-5}
$Im(K_1/k_1)$
c=0.15
0.05
SiC-Aluminum
h/a = 0.0
h/a = 0.1
iterative
0
0.5
1.0
1.5
2.0
k_2a

Figure 7

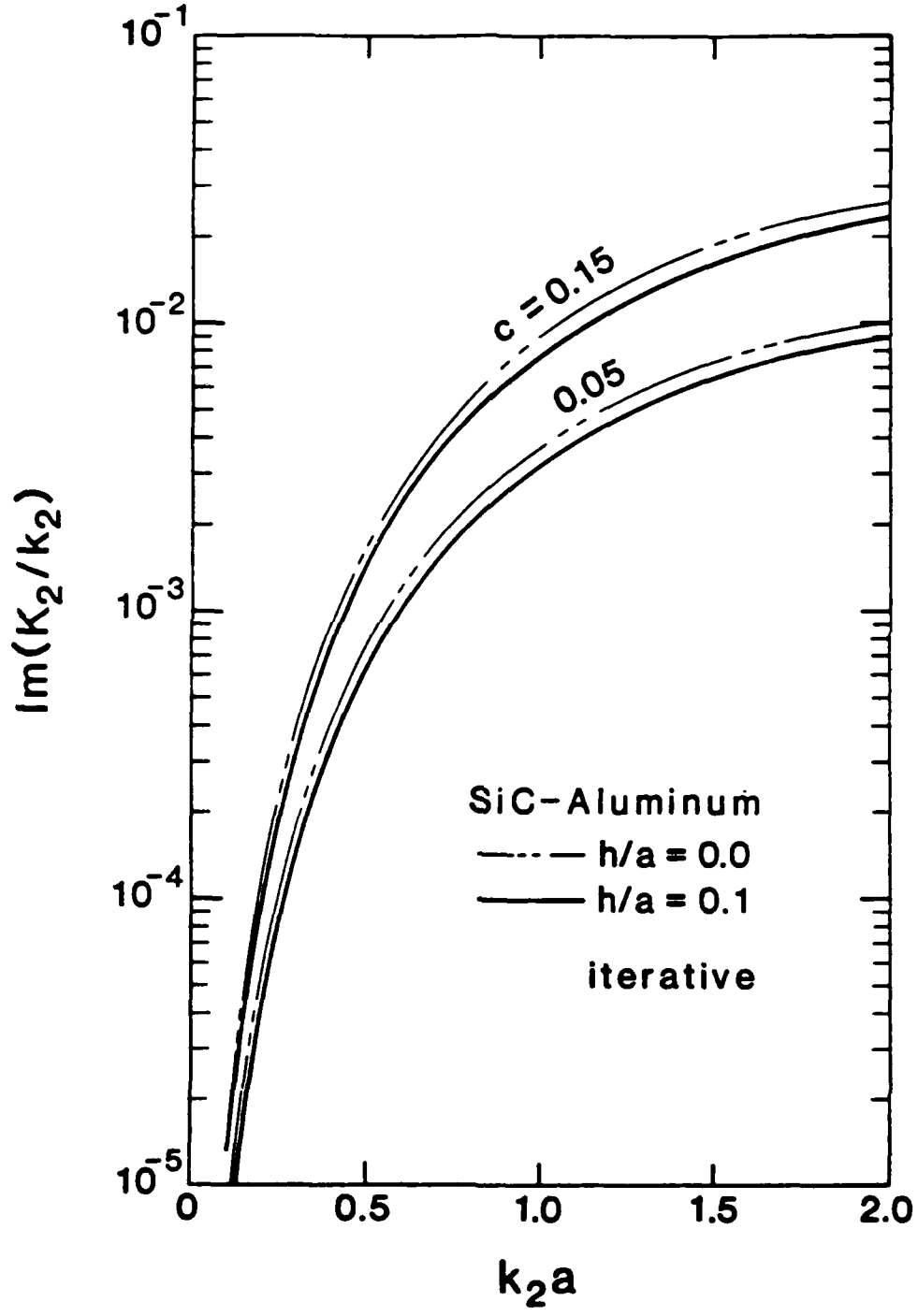
10^{-1}
10^{-2}
10^{-3}
10^{-4}
10^{-5}
$Im(K_2/k_2)$
c = 0.15
0.05
SiC-Aluminum
h/a = 0.0
h/a = 0.1
iterative
0
0.5
1.0
1.5
2.0
k_2a

Figure 8

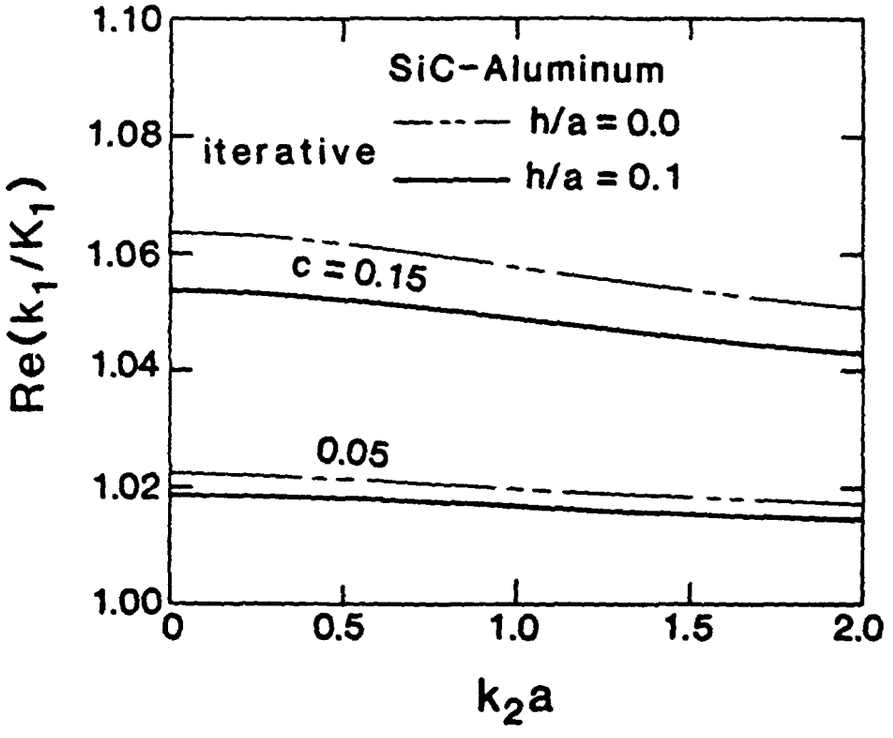
SiC-Aluminum
h/a = 0.0
h/a = 0.1
iterative
c = 0.15
0.05
1.10
1.08
1.06
1.04
1.02
1.00
0
0.5
1.0
1.5
2.0
Re(k1/K1)
k2a

Figure 9

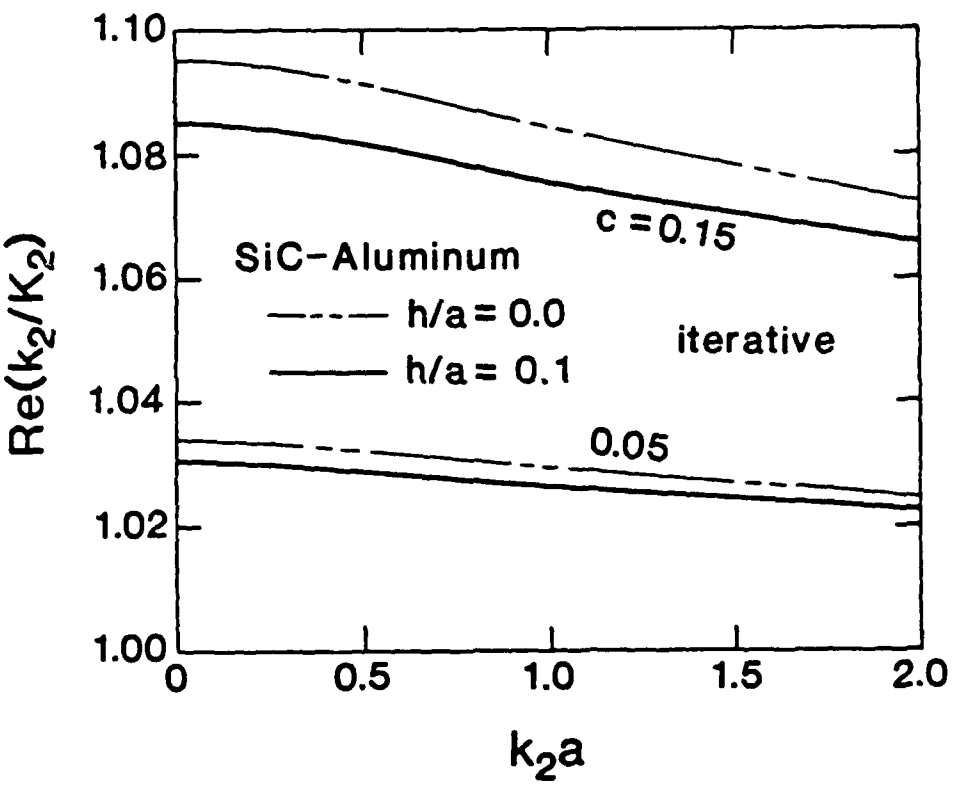
1.10
1.08
1.06
1.04
1.02
1.00
0
0.5
1.0
1.5
2.0
Re(k2/K2)
k2a
SiC-Aluminum
h/a = 0.0
h/a = 0.1
iterative
c = 0.15
0.05

Figure 10

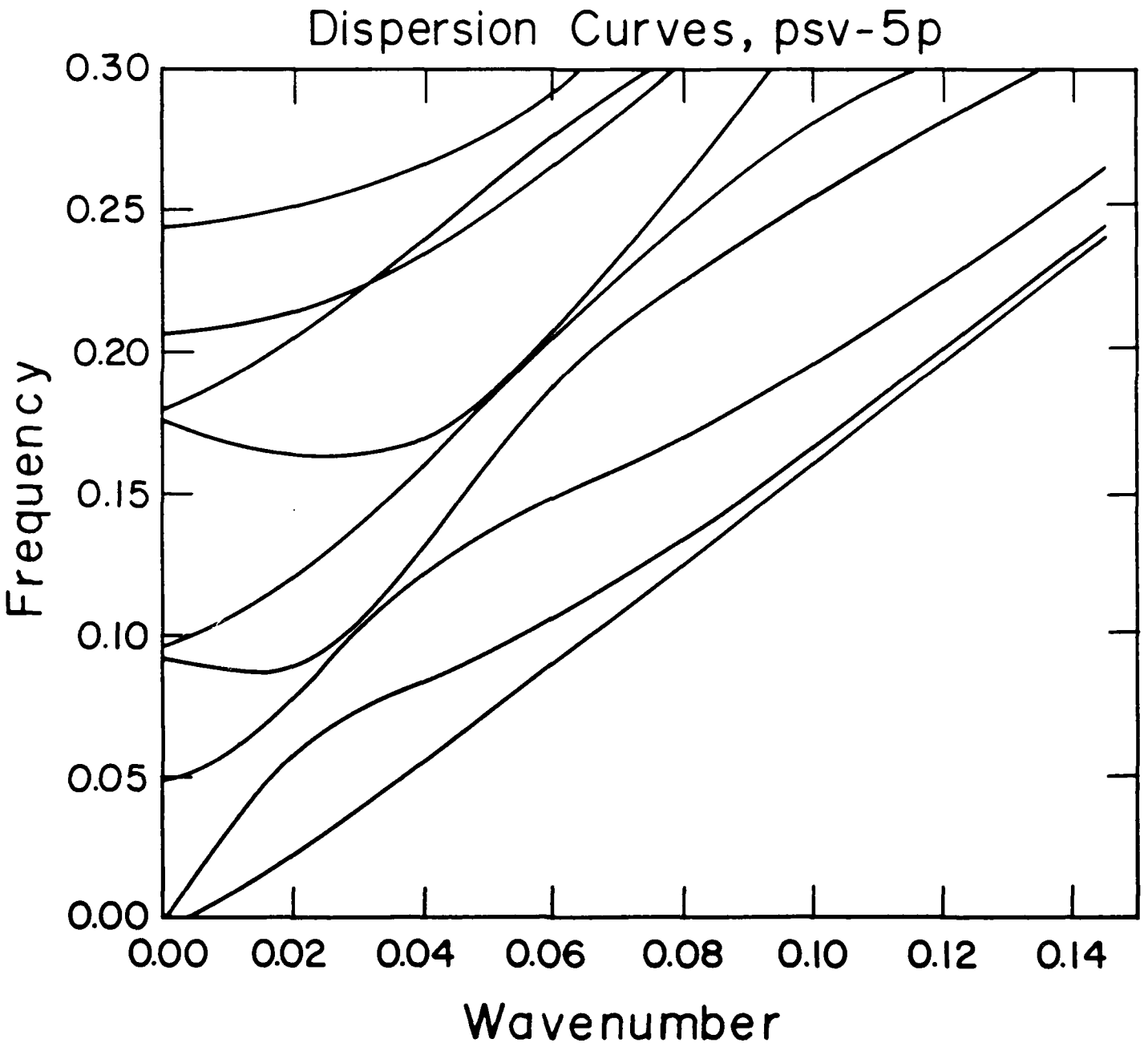
Dispersion Curves, psv-5p
0.30
0.25
0.20
0.15
0.10
0.05
0.00
Frequency
0.00
0.02
0.04
0.06
0.08
0.10
0.12
0.14
Wavenumber

Figure 11

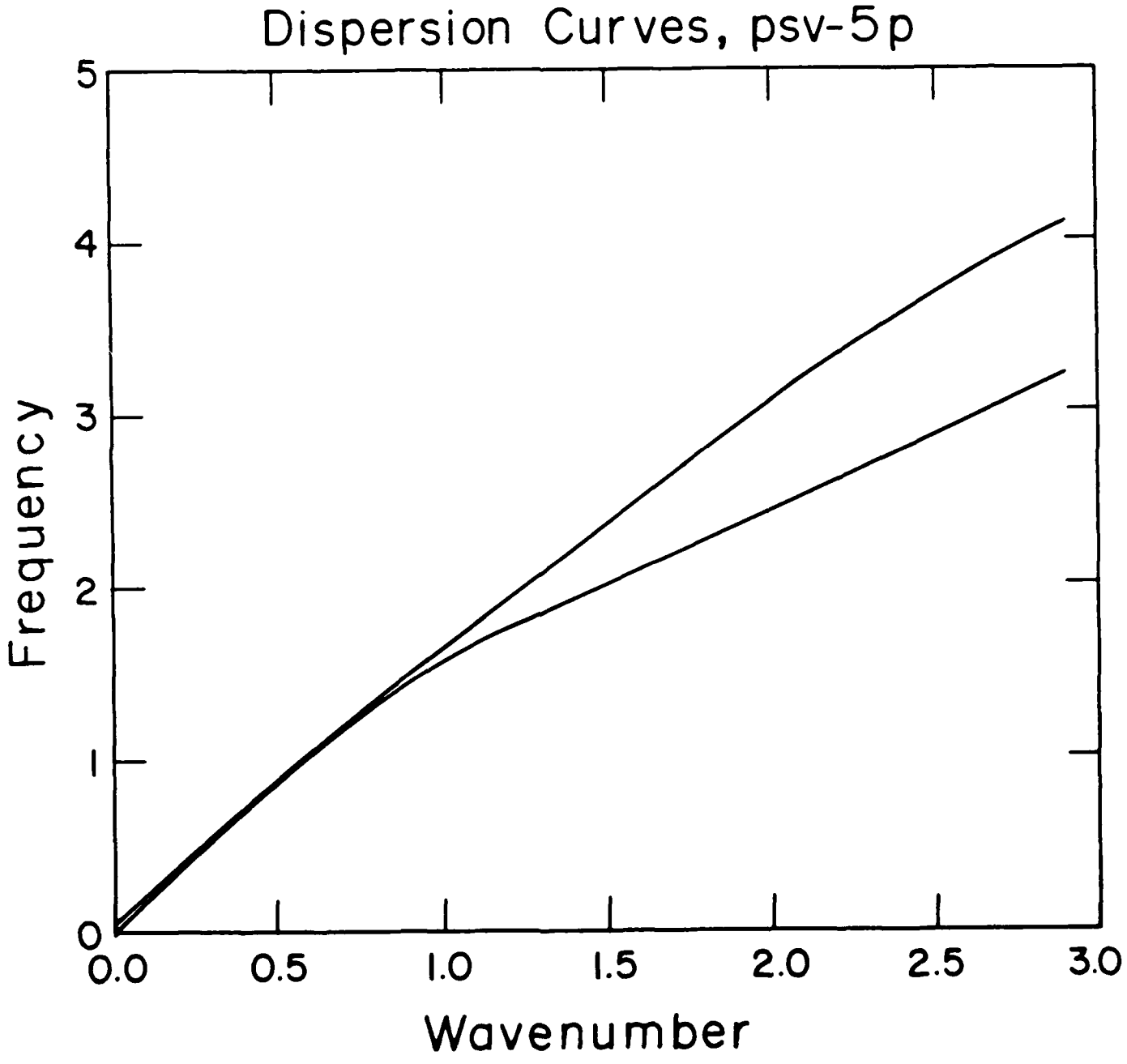
Dispersion Curves, psv-5p
Frequency
Wavenumber
0
1
2
3
4
5
0.0
0.5
1.0
1.5
2.0
2.5
3.0

Figure 12

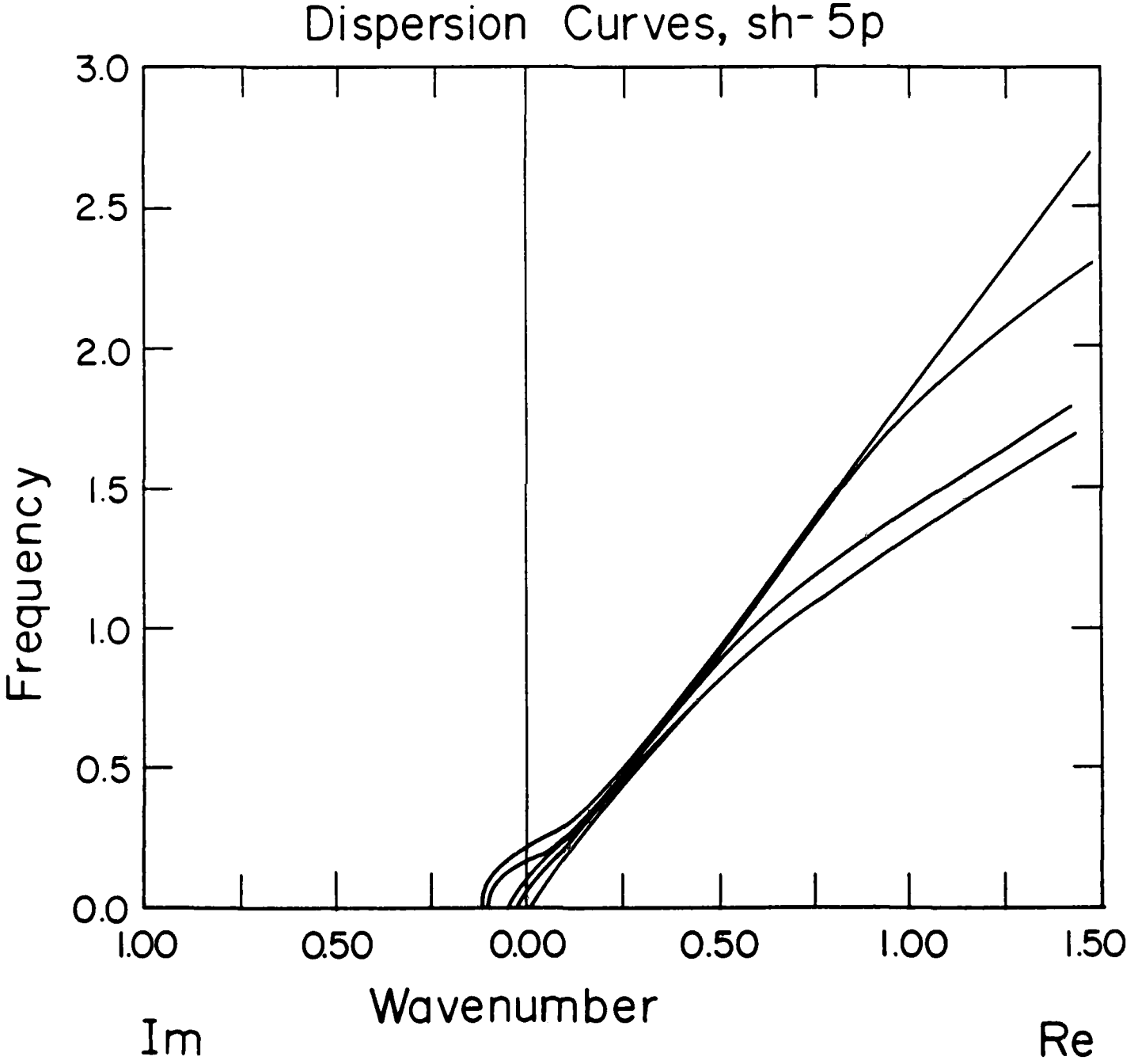
Dispersion Curves, sh- 5p
3.0
2.5
2.0
1.5
1.0
0.5
0.0
Frequency
1.00
0.50
0.00
0.50
1.00
1.50
Wavenumber
Im
Re

Figure 13

END
DATE
FILMD
3-88
DTIC